THE RELATIONSHIP BETWEEN RADAR SCATTERING AND SURFACE ROUGHNESS OF LUNAR VOLCANIC DOMES. E.R. Jawin[1], W.S. Kiefer[2], B. Bussey[3], J.T. Cahill[3], M.D. Dyar[1], C.I. Fassett[1], S. Lawrence[4], P.D. Spudis[2], [1]Astronomy Department, Mount Holyoke College, 50 College Street, South Hadley, MA 01075 (jawin22e@mtholyoke.edu), [2]Lunar and Planetary Institute, Houston, TX, [3]Applied Physics Laboratory, Laurel, MD, [4]Arizona State University, Tempe, AZ.

Introduction: Understanding the morphology of volcanic features on the Moon provides constraints on their emplacement mechanisms. Terrestrial lava flows have been studied using radar imaging in an attempt to distinguish differing flow morphologies. For example, SIR-B radar data taken over the Kilauea Volcano in Hawaii have shown it is possible to distinguish rough a'a from smoother pahoehoe flows, as well as deposits of pyroclastic ash [1]. As on Earth, it is likewise possible to use radar to distinguish different volcanic terrains on the Moon. Rugged lava flows on the Moon such as that in Mare Serenitatis have been identified using Earth-based radar; it has also been used to identify pyroclastic deposits by their low backscatter and CPR in Mare Vaporum and southern Mare Serenitatis [2]. By observing areas of distinct backscatter and circular polarization ratio (CPR), it is possible to infer their original flow morphologies [3].

In this work, we explore the relationship between surface roughness and the radar signatures of various lunar volcanic domes, as well as other lunar geologic features. In order to quantify this relationship, we have compared radar CPR values at S- and P-band wavelengths (12.6 and 70 cm, respectively) with RMS topographic variation attained from Lunar Orbiter Laser Altimeter (LOLA) data. These different parameters describe roughness on a range of length scales.

Several regions on the Moon were chosen for analysis using this technique: volcanic domes include the Marius Hills domes [4, 5, 6], the Gruithuisen and Mairan domes [7], as well as the Rümker Hills volcanic complex [5]; a suite of other features were analyzed, including various mare basalt lava flows, pyroclastic dark mantle deposits (DMD's) [2, 8], rough lava flows in Mare Serenitatis [3], and the ejecta blankets and floors of the large, fresh craters Copernicus and Tycho.

Methods: *LOLA Data: RMS Misfit and Pulse Width.* LOLA measures the Moon's topography. Each sequential shot containing five points arranged in a cross pattern is separated by ~57 m, while the smallest point-to-point baseline is ~25 m [9]. We used LOLA data [10] to calculate RMS topographic meter-scale roughness to compare with CPR data. To do this, a MATLAB script was used to group three successive LOLA shots together and use the spot data to create a least-squares plane. In this script, all invalid data points were removed from the data set [10]. To ensure valid least squares planes, we only generated data if there were at least nine valid returns; if all three successive spot patterns were receiving data, there were a total of fifteen data points (results typically included 14-15 points on each calculated plane). This plane was then used to calculate the RMS misfit of each data point from the plane, which represents the roughness of the lunar surface on a 25-50 m scale.

Along with topography, LOLA also measures the time interval of each returned laser pulse, referred to as pulse width [10]. This interval is controlled by the small-scale topographic roughness within each 5 meter diameter measurement spot, with rougher topography causing the returned pulse to be broadened in time. The pulse widths are the averages for each study area and are reported in terms of the measured time interval in nanoseconds. Measured pulse widths for our study regions range between 12 and 25 nsec, with larger values corresponding to rougher terrain within the 5 meter diameter laser spot. A more quantitative analysis of the relationship between pulse width and surface roughness, paralleling Neumann et al.'s study [11] of martian altimetry, is in development.

Radar Data: CPR. The radar systems used in this study transmit in circular polarization. When an incident beam reflects off a surface, it changes the sense of polarization to the opposite of that transmitted (OC); likewise, if the beam reflects off two objects, it reverses polarization twice, therefore resulting in the same sense of which it was transmitted (SC). The circular polarization ratio (CPR) is the ratio of received power in the same sense to opposite sense transmitted (SC/OC) [12]. Rough, blocky surfaces have the potential to cause incident radar beams to bounce more than once, leading to more SC signals and thus high CPR; therefore, rougher surfaces show higher mean CPR. Additionally, depending on the radar wavelength and the composition of the regolith, it is possible to observe features below the surface [5]. The probing depth of the radar is a function of wavelength – S-band wavelength (12.6 cm) can penetrate up to a meter or two in typical mare regolith, while P-band wavelength (70 cm) is sensitive to depths about five times greater, making it possible to observe rocks suspended in the regolith at different depths [5]. Likewise, S-band signals are sensitive to surface and suspended rocks ~2 cm and larger, while P-band signals are sensitive to rocks ~10 cm and larger [5]. By comparing the rough-

ness on small scales from CPR to larger-scale roughness from RMS misfit (referred to here as RMS topographic roughness) and pulse width, we hope to gain an understanding of the large- and small-scale topography of a suite of lunar features.

CPR values were collected for the various geological features at both S- and P-band wavelengths. Using the image processing programs ISIS and ArcMap, we extracted CPR values made by the Mini-RF spacecraft on the Lunar Reconnaissance Orbiter [12]. Radar results were measured at the same study regions as the altimetry.

Results: Our results are summarized in Figures 1 and 2. Each symbol is the average of all results calculated in a 6 x 6 km study area. There are typically at least three data points from each geographic region.

Values for RMS topographic roughness, pulse width and CPR were plotted against each other in order to observe their dependences. When S-band CPR values were plotted against topographic roughness (Figure 1), there was an apparent correlation. As expected, lava flows and DMD's had the lowest CPR and topographic roughness, while the various domes had intermediate values, and crater features had the highest CPR and topographic roughness overall.

The point-to-point topographic roughness and pulse width (figure not shown) show a weaker positive correlation. The crater units are roughest at both scales, and the mare flows and DMD's are smoothest on both scales. However, the Gruithuisen and Mairan domes have distinctly higher pulse width than the Marius Hills domes, despite similar topographic roughness at longer wavelengths, possibly reflecting a different emplacement style and/or magma composition.

P-band CPR plotted against pulse width (Figure not shown) follows a similar linear relationship; mare lava flows and the Rümker Hills had low CPR and topographic roughness, while crater features and the Marius Hills had higher values for both.

A comparison of P-band and S-band CPR values (Figure 2) shows an analogous linear correlation between the low-CPR mare lava flows and Rümker Hills, and the higher-CPR crater features and Marius Hills domes. However, data collection is ongoing and incomplete.

The Marius Hills domes show a wide variation in P-band CPR values, between 0.37-0.91. The range of values for individual domes may be due to dome age, size, or geology. Further research may clarify the possible source(s) of this variation.

References: [1] Gaddis, L.R. et al., (1989) *GSA-B, 101,* 317-332. [2] Carter, L.M. et al., (2009) *JGR, 114,* E11004. [3] Campbell, B.A. et al., (2009) *GRL, 36,* L22201. [4] Besse, S. et al., (2011) *JGR, 116*, E00G13. [5] Campbell, B.A., Hawke, B.R., and Campbell, D.B. (2009) *JGR, 114,* E01001. [6] Lawrence et al., (2010) *LPSC 42*, abstract 2422. [7] Wilson, L. and Head, J.W. (2003) *JGR, 108, NO. E2*, 5012. [8] Head, J.W. (1974) *Proc. LPS V,* 207-222. [9] Rosenburg, M.A. et al., (2011) *JGR, 116,* E02001. [10] Smith, D.E. et al., (2010) *GRL, 37*, L18204. [11] Neumann, G.A. et al., (2003) *GRL, 30, NO. 11, 1561*. [12] Raney, R.K. et al., (2011) *Proc. IEEE*, 99, 5.

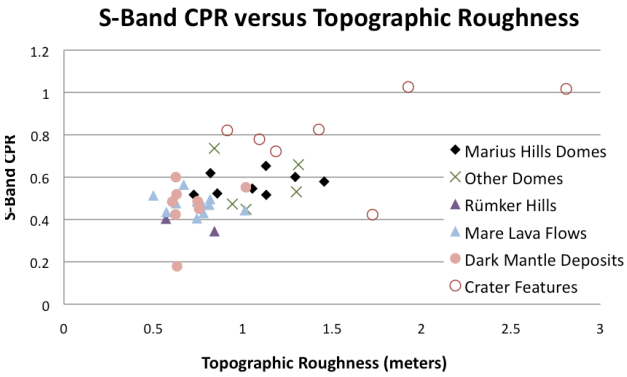

Figure 1. S-band (12.6 cm) circular polarization ratio plotted against topographic roughness

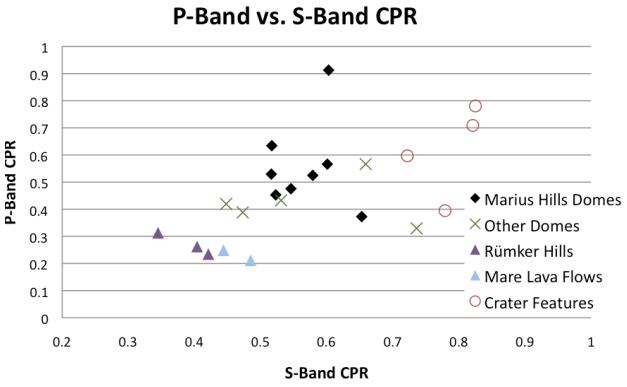

Figure 2. P-band (70 cm) circular polarization ratio plotted against S-band (12.6 cm) circular polarization ratio